추진제의 마이크로 스케일 상면 두께 예측

여재익*

Predicting Micro-Thickness of Phase Fronts in Propellants

Jai-ick Yoh*

ABSTRACT

I consider the structure of steady wave system which is admitted by the continuum equations for materials that undergo phase transformations with exothermic chemical reaction. In particular, the dynamic phase front structures between liquid and gas phases, and solid and liquid phases are computationally investigated. Based on the one-dimensional continuum shock structure analysis, the present approach can estimate the nano-width of waves that are present in combustion. For illustration purpose, n-heptane is used in the evaporation and condensation analysis and HMX is used in the melting and freezing analysis of energetic materials of interest. On-going effort includes extension of this idea to include broad range of liquid and solid fuels, such as rocket propellants.

초   록

이 논문은 발열 반응에서 상이 변화하는 물질의 연속 방정식에서 유도되는 안정된 파면의 구조를 고려했다. 특별히 액체와 기체, 고체와 액체 사이의 동적인 파면 구조를 수치적으로 연구하였다. 1차원 충격파 구조 분석에 근거한 본 연구에 의하면 연소 시 나노 사이즈의 파면이 존재한다고 추정한다. 설명을 위해, 증발과 응축에는 n-heptane이 사용되었고, 용해와 응고에는 HMX를 사용하였다. 이 개념의 확장은 로켓 추진제와 같이 액체, 고체 연료의 넓은 범위 모두를 포함한다.

Key Words: Phase-Field Model, Energetic Materials, Thermo-Mechanical Modeling, Melting, Freezing, Evaporation, Condensation, Numerical Integration

1. Introduction

In the continuum theory, a shock is interpreted as a thin region, rather than a discontinuity, in which rapid changes of the flow quantities occur. Two uniform end states of a typical shock are related through a smooth structure of finite length in microns where the conservation of mass, momentum and energy is achieved. In this article, a new

* 서울대학교 기계항공공학부
  연락저자, E-mail: jjyoh@snu.ac.kr

method of calculating the thickness of the phase fronts that propagate in much the same way as a shock wave in a continuous media.

A thermo-mechanical model for energetic materials [1] is used in the analysis of wave structures that exist between different phases. In particular, the liquid-vapor interface that moves with the phase transformation (evaporation and condensation) is analyzed. The phase front of solid-liquid interface is also analyzed with the model equations of energetic materials that is referenced in [1]. For evaporation and condensation of energetic materials, n-heptane liquid fuel is considered while an HMX is chosen for illustration of the wave structure associated with melting and freezing.

The shocked state is the unstable equilibrium. The integration of the structure starts from this point to a stable point of unshocked state. Figure 1 shows a steady shock coordinate where $\xi = x - Dt$, $U = u - D$ so that in this frame, velocities both upstream and downstream are negative, pointing left. Here D is the steady wave speed, directed in the negative ξ direction (i.e. $D<0$). The derivatives with respect to x and t become

$$\frac{\partial}{\partial t} = \frac{\partial \xi}{\partial t}\frac{d}{d\xi} = -D\frac{d}{d\xi}; \frac{\partial}{\partial x} = \frac{d}{d\xi} \qquad (1)$$

and, the velocity gradient becomes

$$\frac{\partial u}{\partial x} = \frac{dU}{d\xi} \qquad (2)$$

Thus the equations of motion for the ideal gas are as follows:

$$\rho U = m, \ (U = D - u)$$
$$\frac{dU}{d\xi} = \frac{3}{4\mu_f}\left\{mU_{-\infty} + \frac{m}{U_{-\infty}}RT_1 - mU - \frac{m}{U}RT\right\}$$
$$\frac{dT}{d\xi} = \frac{1}{K}\left\{\begin{array}{l}\frac{\gamma}{\gamma-1}mRT_1 + \frac{1}{2}mU_{-\infty}^2 - \frac{4}{3}\mu_f UU_\xi \\ -\frac{\gamma}{\gamma-1}mRT - \frac{1}{2}mU^2\end{array}\right\}$$
$$(3)$$

where $m = \rho U$ and $p = \rho RT$. Using the constants standard of air, such that $\mu_f = 1.95 \times 10^{-5}$ Ns/m^2, $K = 0.0276$ W/m K, and $R = 287$ m^2/s^{2}K, one can integrate from a shocked state into an unshocked state, namely the ambience.

In the following section, the wave thickness of classical phase transformation fronts are calculated much the same was as in the classical shock structure analysis discussed. With careful handling of the model with accurate material data, qualitatively reliable measurement of nano-width of phase fronts is possible using this approach.
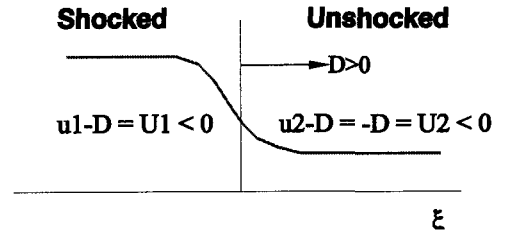

Fig. 1 Schematic of shock-attached frame

2. Structure of Phase Front

Two uniform end states of a typical phase front are related through a smooth structure of finite length in fractions of a micron where the conservation of mass, momentum and energy is achieved. Resembling the structure of a classical shock wave of gas dynamics, evaporation - condensation front and melting - freezing front are carefully studied in the case of transitions between two uniform end states. An estimated thickness of evaporation - condensation front of n-heptane is on the order of 10^{-2} micron while the HMX melting - freezing front thickness is 'measured' at 1 micron.

2.1 Evaporation and condensation front

The details of wave structure between the end states at $\pm\infty$ are provided by transforming the unsteady equations to the steady flow equations in a frame of reference moving with the wave using $\xi = x - Dt$, $U = u - D$. Here D is the steady phase front 'wave' speed, directed in the negative ξ direction (i.e. $D<0$). The derivatives with respect to x and t and the velocity gradient $\partial u/\partial x$ are defined as before (see Eqns. 1 and 2).

The mass and momentum equations transform as follows:

$$\rho U = m \tag{4}$$
$$\rho U \frac{dU}{d\xi} = \frac{d}{d\xi}\left(\sigma + \frac{4}{3}\mu_f \frac{dU}{d\xi}\right)$$

Since the wave structure is of interest, the momentum equation is integrated once with respect to ξ to arrive at a first-order ODE in the form

$$m U - \sigma - \frac{4}{3}\mu_f \frac{dU}{d\xi} = \beta \tag{5}$$

where β is a constant of integration which can be evaluated as $\xi \to -\infty$. With mass flux defined constant, m, the structure momentum equation reads

$$\frac{dU}{d\xi} = \frac{3}{4\mu_f}\{m U + p + \rho\mu_\varphi G^2 - m U_k - p_k\} \tag{6}$$

As for the energy and phase-field structure equations, the partials with respect to x and t are replaced with the derivative in ξ, and the total derivative $\dot\phi$ transforms to $U d\phi/d\xi$ where ϕ is either T or φ. In order to write the energy equation with the highest derivative in first-order, a new variable H is introduced such that the energy equation reads

$$\frac{dH}{d\xi} = \frac{1}{\kappa}\left\{\begin{array}{l} m c_v H - \frac{4}{3}\mu_f\left(\frac{dU}{d\xi}\right)^2 + \rho R T \frac{dU}{d\xi} - B_\varphi(UG)^2 \\ -\rho T \beta_v'(\varphi)\frac{Q_v}{T_v}UG + \rho c_v' T \ln\frac{T}{T_k} \\ + \beta_v'(\varphi) Q_k \end{array}\right\} \tag{7}$$

where H is defined $\frac{dT}{d\xi} = H$, and the index k equals one in the evaporation case and two in the condensation case. As for the phase equation, a variable G is introduced such that

$$\frac{dG}{d\xi} = \frac{1}{\mu_\varphi}\left\{\begin{array}{l} UB_\varphi G + \frac{1}{2}\Psi\frac{\partial}{\partial\varphi}(\varphi(\varphi-1)(\varphi-2))^2 \\ + \beta_v'(\varphi)\frac{T - T_v}{T_v}Q_v \\ - c_v'(T\ln\frac{T}{T_k} - (T - T_k)) \end{array}\right\} \tag{8}$$

with G defined $\frac{d\varphi}{d\xi} = G$.

Note the dependence of c_v, R, and β_v on the phase field variable φ. This generalization of phase dependent coefficients brings in an added complexity to the equations with their derivatives becoming non zero. The choice of φ-dependent coefficients conforms the structure of evaporation wave. In other words, the φ-dependence is introduced in the form of

$$\alpha(\varphi) = \frac{1}{2}\left[\begin{array}{l} \alpha_1\left\{\tanh(\frac{\varphi^* - \varphi}{\epsilon}) + 1\right\} \\ + \alpha_2\left\{\tanh(\frac{\varphi - \varphi^*}{\epsilon}) + 1\right\} \end{array}\right] \tag{9}$$

whose derivative with respect to φ is

$$\alpha'(\varphi) = \frac{1}{2\epsilon}\alpha_2 \operatorname{sech}^2\left(\frac{\varphi - \varphi^*}{\epsilon}\right) - \frac{1}{2\epsilon}\alpha_1 \operatorname{sech}^2\left(\frac{\varphi^* - \varphi}{\epsilon}\right) \tag{10}$$

Here, α can be any of $c_v, c_p, \beta_v, \beta_m$, or R with appropriate end states specified. φ^* is $(3+\sqrt{3})/3$ for vaporization/condensation and $(3-\sqrt{3})/3$ for melting/freezing. With ϵ chosen intelligently, the resulting transport function works like a switch between the two end states. With these switch functions, one

can proceed to solve the governing equations, after specifying all other parameters relating the properties of n-heptane as listed in Table 1.

The integration of these autonomous ODE's, is performed with the high-order Runge-Kutta scheme [2] to march in ξ. In the case of evaporation, the liquid state at $k=1$ (i.e. $\xi = -\infty$) is fixed with the following set of quantities:

Table 1 Dimensional parameters for n-heptane evaporation and condensation

Property	Value
c_v^{liquid}	2.136×10^3 J/kg K
c_v^{vapor}	2.136×10 J/kg K
R_{liquid}	3 J/kg K
R_{vapor}	3×10^2 J/kg K
$\mu_{f-liquid}$	5.4×10^{-4} kg/m s
$\mu_{f-vapor}$	5.4×10^{-4} kg/m s
B_φ	3.5×10^{-2}
μ_φ	2.0×10^{-12}
Ψ	40.0×10^{-6}
$T_{vaporization}$	371.4 K

$(\rho_1=675$ kg/m^3, $m=0.7315515$ kg/m^{2}s, $D=1.08378e-3$ m/s, $u_1=0$ m/s, $T_1=300$ K, $p_1=6.07500e5$ Pa, $\varphi_1=1.0000001$, $H=G=0$, $Q_1=+3.35e15$ J) at $\xi=-\infty$

The numerical integration starts from state 1 (liquid side) at $-\infty$ to state 2 (gas side) at $+\infty$. Figures 2 and 3 represent the structure of evaporation wave admitted by the equations. As the initial state is perturbed, the solution of the equation is described by the integration path, going through a particular structure-stable point on the far right side.

The velocity profile (though not shown) is such that the initial value of 10^{-3} m/s jumps to become 10^{-1} m/s positioned at a stable state where the density jump corresponds to an

n-heptane evaporation case [3-5]. As the phase-field variable changes from 1 to 2, the thickness of the phase front measures on the order of ten nano-meters.

Considering an experimentally measured thickness of similar waves in helium on the orders of millimeters [6], the suggested evaporation front thickness is much smaller. At each end, the temperature gradient is uniform so that $T(-\infty)$ is constant and $T(+\infty)$ is linear with respect to ξ, representing a far-field constant thermal-gradient condition for evaporation process.
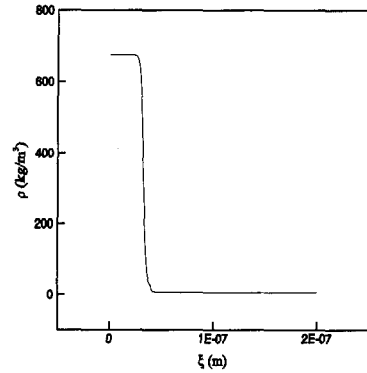

Fig. 2 Evaporation wave structure based on the density field of n-heptane.

In the case of condensation, the vapor state-2 is fixed at $-\infty$, and the integration extends to the liquid state at $+\infty$. The initial conditions of integration for condensation are as follows:
$(\rho_2=5$ kg/m^3, $U_2=0.11$ m/s, $m=0.7315515$ kg/m^{2}s, $T_2=480$ K, $\varphi_2=1.9999991$, $H=G=0$, $Q_2=-4.35e14$ J) at $\xi=-\infty$
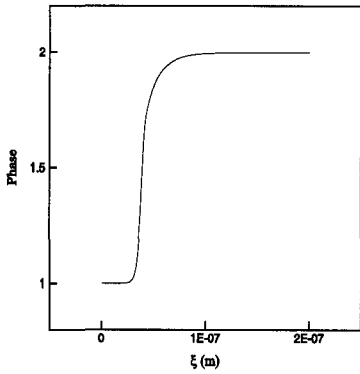
Fig. 3 Evaporation wave structure based on the phase field of n-heptane.
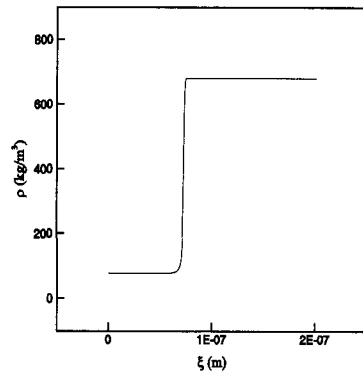

Fig. 4 Condensation wave structure based on the density field of n-heptane.

Here, the integration is reversed from the fixed state at $k = 2$ to a new state at $k = 1$. Figures 4 and 5 represent the structure of condensation wave admitted by the solution of the equations described with $k = 2$. The structure is nearly identical to that of evaporation, except the direction of integration is reversed. With a suitable value for the heat of condensation, Q, the integration starts from a vapor to a liquid zone through a thin region of ten nano-meters. The density profile in Fig. 4 resembles an experimental observation of fuel-droplet condensation; the end state density is about 675 kg/m^3, prototypical of hydrocarbon liquid fuel [4,7]. While the reverse heat is added to drive the vapor state back to a liquid, the far end state temperature gradients remain uniform, such that $T(-\infty)$ is constant and $T(+\infty)$ is linearly decreasing with respect to ξ.
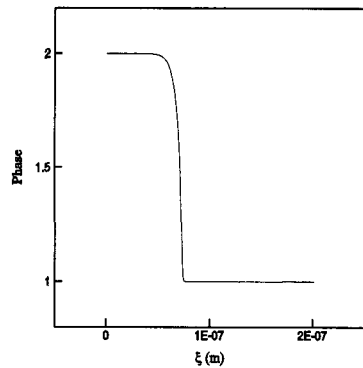

Fig. 5 Condensation wave structure based on the phase field of n-heptane.

2.2 Melting and freezing front

The structure equations, in the case of solid to liquid or liquid to solid transition, are obtained in analogy to the previous case of evaporation - condensation. Main distinction in the equations is the added dependency of conservative variables on the deformation field. A variable, F, is the one-dimensional deformation gradient which is introduced into

the momentum, the energy, and the phase-field equations. Again with mass flux remaining a constant, m, the momentum structure equation, after integrated from $-\infty$ to a position in ξ, becomes

$$\frac{dU}{d\xi} = \frac{3}{4\mu_f}\left\{\begin{array}{l} mU + p + \rho\mu_\varphi G^2 - \mu_s F \\ + \mu_l F^{\frac{-1}{1-2\nu_s}} - mU_k - p_k \end{array}\right\}$$

(11)

The equation represents melting if $k=1$ or freezing if $k=2$. The energy equation reads

$$\frac{dH}{d\xi} = \frac{1}{\kappa}\left\{\begin{array}{l} mc_v H - \frac{4}{3}\mu_f\left(\frac{dU}{d\xi}\right)^2 + \rho RT\frac{dU}{d\xi} + \mu_s F\frac{dU}{d\xi} \\ -\mu_l F^{-\frac{1}{1-2\nu_s}}\frac{dU}{d\xi} - B_\varphi(UG)^2 \\ -\rho T\beta'_m(\varphi)\frac{Q_m}{T_m}UG + \rho c'_v T\ln\frac{T}{T_k} \\ +\beta'_m(\varphi)Q_k - \frac{1}{2}\mu_s F^{-1}(F^2-1)(UG) \\ -\frac{1-2\nu_s}{2\nu_s}\mu'_l F^{-1}(F^{-\frac{2\nu_s}{1-2\nu_s}}-1)(UG) \end{array}\right\}$$

(12)

where, like in the evaporation/condensation case, a new variable, H was introduced to split the original energy equation into a set of two first-order ODE's with $\frac{dT}{d\xi} = H$.

Likewise, the phase field equation reads

$$\frac{dG}{d\xi} = \mu_\varphi\left\{\begin{array}{l} UB_\varphi G + \frac{1}{2}\Psi\frac{\partial}{\partial\varphi}(\varphi(\varphi-1)(\varphi-2))^2 \\ +\beta'_m(\varphi)\frac{T-T_m}{T_m}Q_m \\ -c'_v(T\ln\frac{T}{T_k}-(T-T_k)) + \mu'_s\frac{1}{2}F^{-1}(F^2-1) \\ +\mu'_l\frac{1-2\nu_s}{2\nu_s}F^{-1}(F^{-\frac{2\nu_s}{1-2\nu_s}}-1) \end{array}\right\}$$

(13)

with $\frac{d\varphi}{d\xi} = G$. Lastly, we need to close the system with additional equation which relates the deformation gradient field with the

velocity field via the identity $\frac{dF}{d\xi} = -\frac{F}{U_k}\frac{dU}{d\xi}$ or $F = e^{-\frac{U}{U_k}+1}$. We choose HMX as a candidate for solid - liquid structure analysis for which a handful material data is known [8-12]. Table 2 lists the parameters of HMX as needed in the calculation of melting and freezing structure.

In the case of melting, the solid state of HMX is fixed by setting $k=1$ and the following initial conditions at $\xi=-\infty$: (ρ_1=2000 kg/m^3, m=2.0 x 10^3 kg/m^{2}s, D=1.0 m/s, u_1=0 m/s, T_1=300 K, p_1=6.07500e5 Pa, φ_1=0.0000001, F=1.00000001, H=G=0, Q_1=+3.3e14 J) at $\xi=-\infty$

Since there is no data for melting rate of HMX, D is assigned in the range of 10^{-3} to 10^3 m/s. The minimum in this range corresponds to a typical deflagration rate while the maximum corresponds to a typical detonation speed [13-16]. A natural choice is to take the mean value, approximately 1 m/s.

Figure 6 and 7 depict the structure of a melting front admitted by the equations. In particular, the initial density of 2000 kg/m^3, typical of solid explosive, decreases by a factor of two. The system of ODE for melting is integrated from a slightly perturbed initial state into a new state representative of a melt HMX. The thickness of the phase front is on the order of microns, supporting the observation that explosive melting front is approximately hundred times thicker than the evaporation/condensation front of liquid fuel.

The initial state of solid HMX is essentially unstressed (i.e. F=1) while the end state of the integration is at a compression state at $F \sim 0.3$. In fact, the wave, a compression wave, on the far right side, propagates into an

unstressed material on the left side at a steady melting speed of D. This observation is consistent with the principles of energy transfer from a higher state to a lower state. The temperature field (though not shown) also supports this observation that uniform state on the left is balanced by a linearly increasing thermal field on the far right, causing the energy transfer to go from liquid to solid, essentially a melting process by definition [17-20].
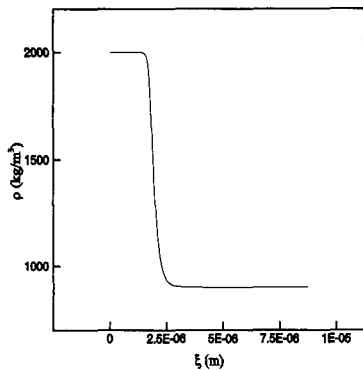

Fig. 6 Melting front structure observed from the density field of solid HMX.

In the case of freezing, the liquid state-2 is fixed at $-\infty$, and the integration starts from the far left in the liquid region to a solid state at $+\infty$. Listed below are the initial conditions of integration for which the liquid state is assumed uniform:

(ρ_2=1580 kg/m^3, U_2=1.4 m/s, m=2.0e3 kg/m^{2}s, T_2=700 K, φ_2=0.9999991, F=1.00000001, H=G=0, Q_2=-4.2e14 J) at $\xi=-\infty$
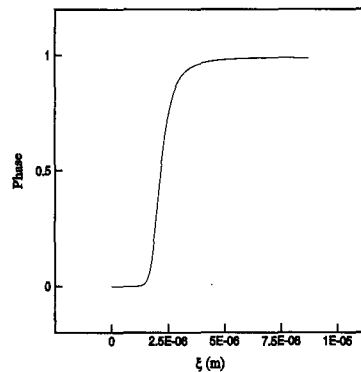

Fig. 7 Melting front structure observed from the phase field of solid HMX.

Figures 8 and 9 represent the structure of a freezing front, admitted by the equations just described with setting $k=2$. Previous investigation of thermodynamic properties of HMX suggests that the material can undergo a liquid-solid transition at a temperature 550 K and a pressure above 50 x 10^5 Pa. So the process of 'freezing', in principle, is realizable at this melting temperature with an elevated pressure of 50 x 10^5 Pa or above. typical melt explosive density of 10^3 kg/m^3 makes a rapid transition to a new state, a solid state as shown in Fig. 8. Again, the thickness of numerically obtained freezing front is in the order of microns, which is about hundred times the thickness of condensation front of hydrocarbon liquid fuel. As the phase field changes from 1 to 0, the deformation field goes from an unstressed liquid at $F(-\infty) \approx 1$ to a tensional state at $F(+\infty) \approx 1.3$. The front again moves from right to left with a steady propagating speed of $D \approx 1.26$ m/s.

Table 2 Dimensional parameters for HMX melting and freezing

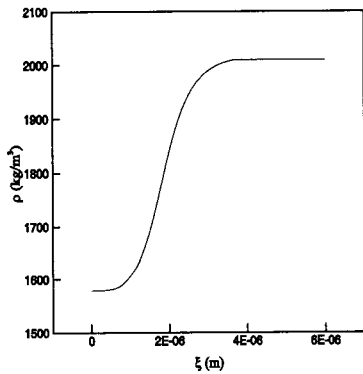| Property	Value
c_v^{solid}	1.06×10^3 J/kg K
c_v^{liquid}	2.1×10^3 J/kg K
R_{solid}	1.1 J/kg K
R_{liquid}	3.0 J/kg K
$\mu_{f-solid}$	1.0×10^{-3} kg/m s
$\mu_{f-liquid}$	1.0×10^{-3} kg/m s
B_φ	3.5×10^{-2}
μ_φ	2.0×10^{-12}
Ψ	40.0×10^{-6}
$T_{melting}$	558 K

Fig. 8 Freezing front structure observed from the density field of solid HMX.
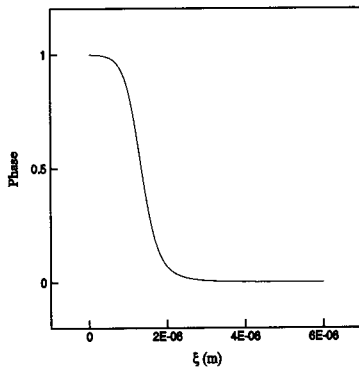
Fig. 9 Freezing front structure observed from the phase field of solid HMX.

3. Conclusions

A thermo-mechanical model for energetic materials that undergo phase transformation is reconstructed to understand the structures of waves that are present in combustion. In particular, the thickness of evaporation and condensation phase fronts are analysed by integrating the structure equations of *n*-heptane from one state to the other. The thickness estimation of melting and freezing waves are illustrated by considering HMX as an energetic material undergoing phase transformation. Based on the analysis, the phase front width of liquid-gas or gas-liquid phase (of, say, a liquid fuel) is approximately one hundredth of the calculated width of solid-liquid or liquid-solid phase front of high explosive. Though not fully generalized at this stage, the approach illustrated in this article can be extended to phase front thickness estimations of other matters where the experimental measurements are not attainable. Other use of this technique may include size estimation of small scale device where melting and evaporation of a fuel exist during the normal operation of the device.

4. References

1. 여재익, "로켓 추진제의 고체-액체-기체 상변화 모델링 연구," 군사과학기술학회 종합학술대회 논문집, 서울대학교, 2005
2. J. J. Yoh, and X. Zhong, "New Hybrid Runge-Kutta Methods for Unsteady Reactive Flow Simulation," AIAA Journal,, 42, pp. 1593-1600, 2004.
3. W. A. Sirignano, "Fluid Dynamics and Transport of Droplets and Sprays," Cambridge University Press, 1999.

4. C. K. Law, "Recent Advances in Droplet Vaporization and Condensation," Progress in Energy and Combustion Science, 88, pp. 171-201, 1982

5, J. S. Shuen, V. Yang, and C. C. Hsia, "Combustion of Liquid-Fuel Droplets in Supercritical Conditions," Combustion and Flame, 89, pp. 299-319, 1992

6. P. A. Thompson, "Compressible-Fluid Dynamics," Advanced Engineering Series, 1988.

7. J. Timmermans, Physico-chemical Constants of Pure Organic Compounds, v.1, 2, New York: Elsevier Publishing Co., 1965

8. T. L. Boggs, "The Thermal Behavior of Cyclotrimethylenetrinitramine (RDX) and Cyclotetramethyleneteranitramine (HMX)," Progress in Astro. and Aero., 90, pp. 121-175, 1984

9. B. M. Dobratz and P. C. Crawford, LLNL Explosive Hand Book, Lawrence Livermore National Laboratory, 1985

10. J. M. Rosen and C. Dickinson, "Vapor Pressures and Heats of Sublimation of Some High Melting Organic Explosives," Journal of chemical and Engineering Data, 14, pp. 120-124, 1969

11. J. W. Taylor and R. J. Crookes, "Vapour Pressure and Enthalpy of Sublimation of HMX," Journal of Chemical Society. Faraday Transactions, 72, pp. 73-728, 1976

12. J. J. Yoh and M. A. McClelland, "An Overview of Thermal-Chemical-Mechanical Modeling off HMX-based Explosives," 41st Joint Propulsion Conference, Tucson, AZ, 2005, AIAA-2005-4554

13. W. Fickett and W. C. Davis, Detonation, University of California Press, Berkeley, CA., 1979

14. F. A. Williams, Combustion Theory, Addison-Wesley, 1985

15. R. Strehlow, Fundamentals of Combustion, Kreiger, 1978

16. K. K. Kuo, Principles of Combustion, Wiley-Interscience, 1986

17. F. Reif, Fundamentals of Statistical and Thermal Physics, McGraw-Hill Book Co., 1985

18. A. B. Pippard, Elements off Classical Thermodynamics for Advanced Student of Physics, Cambridge University Press, 1966

19. H. B. Callen, Thermodynamics, John Wiley & Sons Inc., 1985

20. J.-P. Poirier, Introduction to the Physics of the Earth's Interior, Cambridge University Press, 1991